Eur. Phys. J. B **5**, 881–897 (1998)

THE EUROPEAN PHYSICAL JOURNAL B

© EDP Sciences
Springer-Verlag 1998

Entropy-driven polymer collapse: Application of the hybrid MC/RISM method to the study of conformational transitions in macromolecules interacting with hard colloidal particles

P.G. Khalatur[1], L.V. Zherenkova[1], and A.R. Khokhlov[2,a]

[1] Department of Physical Chemistry, Tver State University, Tver 170002, Russia
[2] Physics Department, Moscow State University, Moscow 117234, Russia

Received: 14 April 1998 / Revised: 20 April 1998 / Accepted: 4 June 1998

Abstract. Self-consistent hybrid MC/RISM method is used for calculating properties of a linear polymer surrounded by colloidal particles with purely repulsive, hard-core, interactions between the particles and chain beads. Our approach combines the traditional atomistic Monte-Carlo (MC) simulation of flexible polymer chains with the numerical solution of the site-site Ornstein-Zernike-like (RISM) integral equations. Since the condensed-phase environment of a flexible macromolecule affects the equilibrium configuration probability distribution of the macromolecule, the site-site intramolecular correlation function and the intramolecular potential field are treated in a self-consistent manner. It is shown that in such an athermal system the medium-induced collapse of a polymer (similar to polymer collapse in a poor solvent) may occur. Our analysis yields a simple "entropic" interpretation of this transition. We present the detailed study of the dependence of conformational properties of the chains on the degree of polymerization, density and size of colloidal particles.

PACS. 02.30.Rz Integral equations – 61.25.Hq Macromolecular and polymer solutions; polymer melts; swelling – 82.70.Dd Colloids

1 Introduction and overview

The understanding of structure and physical properties of polymer-containing colloidal dispersions is important both from theoretical point of view and from the viewpoint of numerous practical applications. Great amount of experimental evidence exists for the effective attraction of colloidal particles induced by small polymeric additives to colloidal dispersions. The effect is well pronounced even in the absence of the adsorption of polymer chains on the surface of particles [1]. The effective attraction between colloidal particles perturbs their homogeneous spatial distribution and, in some of cases, can lead to coagulation (*flocculation*) of a dispersion. It is evident that in the absence of energetic effects the entropy effects must be responsible for the process. In the colloid science, this phenomenon is called *depletion flocculation* [1].

The simplest theoretical models of the depletion flocculation have been considered (see, *e.g.*, Refs. [1–3]). The athermal mixtures of hard-core particles and polymer chains were theoretically studied by Frenkel and coworkers [4,5] (see also the review [6]). Their microscopic approach is based on a recursive scheme that permits calculation of the partition function of an ideal (non-self-avoiding) polymer chain on a lattice in an arbitrary external potential [7,8]. This scheme was used as a starting point to study self-avoiding polymers. According to references [4–8], in the systems with bare hard-core potential there is an effective polymer-induced attraction between the particles. Another approach to the problem under discussion was proposed in our recent work [9], where a microscopic theory of the mixtures of polymer chains and colloidal particles was developed on the basis of the RISM (Reference Interaction Site Model) integral equation technique. It was found that in the athermal regime there is a considerable effective attraction between the small hard-spherical particles in a wide range of polymer number density ρ_p. According to reference [9], at fixed density of colloidal particles ρ_d, the partial reduced compressibility of the dispersed component, $\chi_d^* \equiv k_B T \rho_d \chi_d$, increases rapidly with ρ_p from $\chi_d^* < 1$ to $\chi_d^* > 1$; however, with further increase in ρ_p the value of χ_d^* decreases gradually. As can be shown, in the limit of large ρ_p at $\rho_d \ll 1$ and $N_p \to \infty$ we must have $\chi_d^* \to 1$. This means that the large-scale properties of the dispersed component coincide with those of an ideal reference system. This is due to a complete screening of the bare hard-core potential by long chains in an extremely dense, incompressible and defectless polymer matrix (see also the qualitative arguments of de Gennes [10]). Thus, our approach also confirms the important role

[a] e-mail: khokhlov@polly.phys.msu.su

of the purely entropic (or, in other words, sterical) effects in the problem under consideration.

The problem of entropy-induced effects could be regarded from another viewpoint. We can formulate the following question: how does the medium consisting of hard impenetrable particles affect the equilibrium conformations of a polymer chain? Unfortunately, the version of the RISM-theory developed in reference [9] does not allow us to solve this problem. The point is that the approach used in reference [9] is based on the Gaussian approximation for the intrapolymer pair correlation function, $w_{\alpha\beta}(|\mathbf{r}-\mathbf{r}'|)$, which gives the probability that polymer sites α and β are at a distance $r = |\mathbf{r}-\mathbf{r}'|$. The Gaussian ("ideality") assumption (or the so-called Flory "ideality" postulate) has been demonstrated to be highly accurate for homopolymer melts, where the excluded volume intrapolymer interactions are effectively screened by intermolecular interactions. For dilute (or semidilute) polymer systems, however, large deviations from ideality occur [10], and thus the condensed-phase modification of the intramolecular interactions and the equilibrium conformation must be taken into account. Moreover, the equilibrium polymer conformation and the local arrangement of surrounding particles must be treated in a self-consistent manner.

The structure of binary polymer-containing mixtures may, in principle, be predicted by "direct" computer simulations using Monte-Carlo (MC) or molecular dynamics (MD) methods. However, among all polymer systems the dilute polymer systems with highly asymmetric size ratio $\gamma = \sigma_d/\sigma_p \gg 1$ (σ_p, σ_d = diameters of polymer units and particles) are the most "inconvenient" for direct simulations. The point is that for highly asymmetric mixtures, when the size ratio γ differs considerably from 1, serious ergodicity problems arise, even at $\gamma \approx 3$ [11]. Nevertheless, very recently Monte-Carlo computer simulations of such systems (hard-core, athermal, polymer solutions) were carried out for *lattice* models [12–14]. These simulations presented evidence for the entropy-driven polymer chain collapse in an athermal solvent in the absence of attractive interactions, when the size of solvent particle is larger than the size of polymer links. However, as has been pointed out in reference [14], the situation could, in principle, be different in *continuous* space. The behavior of highly asymmetric off-lattice athermal polymer-containing mixtures, to our knowledge, has not yet been studied in the literature. Thus, work in this direction is of interest. Taking into account the problems of direct off-lattice simulations of such systems, in the present study we will use an extended (*self-consistent*) version of the RISM theory.

The generalization of the RISM approach to the self-consistent calculations of the correlation functions and the medium-induced intramolecular potential has been initiated by Chandler and coworkers [15–17] (see also Refs. [18–30]). This approach was originally developed to study a system of ideal point fermions (which can be viewed as "non-interacting electrons"). It has been shown that there is an analogy between this system and the "conformation" changes of the zero-thickness ideal "polymer". The analogy is based on the fact that in the framework of Feynman's path-integral formalism there is a mathematical isomorphism between a quantum-mechanical solvated electron and a polymer system. It is natural to expect that the behavior of ideal polymers surrounded by massive colloidal particles is similar to that of quantum particles in a classical fluid. As has been found in reference [16], at particular conditions one observes the localization of an excess electron in a hard-sphere fluid; in other words, there is a ground state for an ideal "polymer" in the presence of an external field produced by hard particles. This transition is an entropy-driven one, because there are no attractive forces in the system. Another example of an entropy-driven transition has been studied by Alavi and Frenkel [31]. They considered mixtures of ideal point fermions and atoms (effectively hard spheres) and found evidence for a demixing transition as the chemical potential of the fermions is increased beyond a certain critical value. Using the thermodynamically self-consistent integral equations, Biben and Hansen [32] observed a spinodal instability at high densities for binary hard sphere mixtures with the diameter ratio larger than 5.

The atomistic treatment of dense molecular systems is based on the reference interaction site model integral equation theory [33–35] originally developed for small rigid molecules. In the past, Curro and Schweizer [36–38] proposed an extension of this approach to the equilibrium properties of dense polymer liquids (homopolymer melts). In order to make the application of the RISM theory to the flexible, high polymer liquid mathematically tractable, they assumed that a polymer chain in the melt has a configuration characteristic of a chain in a Θ solvent, *i.e.*, the *intra*chain pair correlation function $w(r)$ satisfies the Gaussian approximation. The method gives fairly good results at high densities of polymer. However, as has been mentioned above, the ideality assumption is not valid in the case of dilute polymer systems. In this situation we employ a combination of direct MC simulation and the numerical solution of RISM integral equations. We will call this approach "the hybrid MC/RISM method". Briefly, the MC technique is applied to generate the configurations of a single chain molecule. Using the coordinates of chain beads, the averaged intrapolymer correlation function is obtained. Then, solving the RISM equations for a given density of colloidal particles, we find the polymer-particle correlation functions. It yields the medium-induced intrapolymer potential and the corresponding effective intramolecular energies, which are used in the standard Metropolis MC procedure. The structural properties of the chain are computed by averaging over the statistically representative set of configurations. As a result of many such iterations, the intramolecular structure is determined self-consistently. Note that the concept of effective medium-induced potential [15–17] has been used to study one-component polymer systems (polymer melts) [24–30]. In the present work, this concept is used to study polymer-containing (bicomponent) colloid systems.

In the next section we give a description of the hybrid MC/RISM scheme for the two-component system

consisting of a flexible polymer chain and hard particles. Here we also outline the pearl-necklace model used to simulate a flexible linear polymer chain. In Section 3, we present our results; their discussion is presented in Section 4. In the final section we summarize the conclusions.

2 Computational procedure

Following Chandler and Andersen [33–35], for an arbitrary one-component system consisting of identical N-atomic molecules we can write the generalized site-site Ornstein-Zernike (SSOZ) or RISM integral matrix equation

$$\mathbf{H}(r)=\int d\mathbf{r}'\int d\mathbf{r}''\mathbf{W}(|\mathbf{r}-\mathbf{r}'|)\mathbf{C}(|\mathbf{r}'-\mathbf{r}''|)[\mathbf{W}(\mathbf{r}')+\rho\mathbf{H}(\mathbf{r}'')]. \tag{1}$$

Here, $r=|\mathbf{r}_\alpha-\mathbf{r}_\beta|$ is the distance between sites (atoms or groups) α and β located on the different molecules interacting *via* the pair potential $u(r)$; ρ is the number density of molecules; $\mathbf{H}(r)$ is the matrix of total *inter*molecular site-site pair correlation functions $h_{\alpha\beta}(r)$; $\mathbf{C}(r)$ is the corresponding matrix of direct correlation functions $c_{\alpha\beta}(r)$; $\mathbf{W}(r)$ denotes the matrix of *intra*molecular site-site distribution functions $w_{\alpha\beta}(r)$; and α, $\beta=1,2,...,N$. For a system of single-site (spherical) particles, *i.e.*, at $N=1$ we have $w(r)=1$. It is natural to consider the colloidal subsystem as a set of spherical particles at a given number density $\rho_d=n_d/V$, n_d being the number of particles in volume V. Thus, using the subscript dd' to identify the corresponding pair correlations and the symbol $*$ to denote integral convolution, we have

$$h_{dd'}(r)=c_{dd'}(r)+\rho_d c_{dd'}(r)*h_{dd'}(r). \tag{2}$$

As to the polymer component, we adopt the approximation made by Curro and Schweizer [36–38]. In this approximation (the so-called PRISM (polymer-RISM) approximation), all sites in a long linear polymer chain are considered as equivalent. In other words, the main idea is to go from partial site-site correlation functions to the collective or preaveraged (molecular) functions (see also Ref. [9]). For example, we can write

$$w(r)=\frac{1}{N}\sum_{\alpha=1}^{N}\sum_{\beta=1}^{N}w_{\alpha\beta}(r), \tag{3}$$

$$h(r)=\frac{1}{N^2}\sum_{\alpha=1}^{N}\sum_{\beta=1}^{N}h_{\alpha\beta}(r). \tag{4}$$

Hence, using the subscripts p and pp' to identify density and molecular correlation functions of the polymer component, we have

$$h_{pp'}(r)=w(r)*c_{pp'}(r)*[w(r)+\rho_d c_{pp'}(r)*h_{pp'}(r)] \tag{5}$$

where $\rho_p=N\rho$ is the monomer number density and ρ is the system number density of N-unit polymer chains.

To take into account correlations of the polymer-particles type, it is necessary to introduce two additional "mixed" total, $h_{dp}(r)$ and $h_{pd}(r)$, and direct, $c_{dp}(r)$ and $c_{pd}(r)$, correlation functions. From the complete set of correlation functions, it is convenient to combine the matrices $\mathbf{H}(r)\equiv[h_{ij}(r)]$ and $\mathbf{C}(r)\equiv[c_{ij}(r)]$, where $i,j=d,p$. In addition we define two diagonal matrices $\mathbf{W}(r)\equiv\mathrm{diag}[w_i(r)]$ and $\mathbf{D}\equiv\mathrm{diag}[\rho_i^{1/2}]$, with $i=d$ or p. We then can write the following integral matrix equation [9,38]

$$\mathbf{DHD}=\mathbf{W}*(\mathbf{DCD})*[\mathbf{W}+\mathbf{DHD}] \tag{6}$$

where $*$ denotes matrix convolution product. Further, we consider the limit of this equation for a polymer "solute" at infinite dilution (*i.e.*, at $\rho_p\to 0$) and obtain the following set of coupled integral equations [9,38]

$$h_{dd'}(r)=c_{dd'}(r)+\rho_d c_{dd'}(r)*h_{dd'}(r) \tag{7}$$

$$h_{pd}(r)=w(r)*c_{pd}(r)*[1+\rho_d h_{dd'}(r)] \tag{8}$$

$$h_{pp'}(r)=w_(r)*c_{pp'}(r)*w(r)+\rho_d w(r)*c_{pd}(r)*h_{dp}(r). \tag{9}$$

With appropriate closure approximation relating the c_{ij} to the h_{ij} we can solve these equations sequentially.

Note that in the approach considered above the low-molecular-weight solvent surrounding both polymer and colloidal particles is treated as a "free volume" and, thus, an effectively two-component description of the three-component system under study is applied.

For a single-site solute in a solvent, the potential of mean force (PMF) between two particles α and β is given by

$$\Psi_{\alpha\beta}(r)=-k_BT\ln[h_{\alpha\beta}(r)+1]. \tag{10}$$

To describe site-site interactions within a polyatomic molecule, we use the two-site-pairwise additive approximation for the total N-site intramolecular solvent-mediated potential $\Delta\Psi$

$$\Delta\Psi(\mathbf{r}_1,...,\mathbf{r}_N)=\sum_{\alpha<\beta}^{N}\Psi_{\alpha\beta}(r) \tag{11}$$

where $\Delta\Psi_{\alpha\beta}(r)$ are the corresponding two-site (pair) components. Note that pairwise additive approximation (11) is applicable to chain molecules with fairly good accuracy [39]. It is even more so if the appropriate model for a chain is employed, namely, the model in which nonoverlaping neighboring beads are well separated along the chain backbone [39].

Considering the behavior of solvated electron, Chandler, Singh, and Richardson [15] (see also Refs. [16–22]) obtained the following solvent-mediated potential

$$\Delta\Psi_{\alpha\beta}(r)=-k_BTc_{\alpha d}(r)*\chi_{dd'}(r)*c_{d'\beta}(r) \tag{12}$$

where $\chi_{dd'}(r)$ is the pure solvent (medium) site density pair correlation function. For the monoatomic medium, $\chi_{dd'}(r)=\rho_d[1+\rho_d h_{dd'}(r)]$, where ρ_d is the bulk density.

Note that potential (12) corresponds to the hypernetted-chain (HNC) closure

$$c(r) = h(r) - \ln[h(r) + 1] - u(r)/k_BT. \quad (13)$$

Recently Grayce and Schweizer [23] proposed a new approximate solvatation potential

$$\Delta\Psi_{\alpha\beta}(r) = -k_BT \ln[1 + c_{\alpha d}(r) * \chi_{dd'}(r) * c_{d'\beta}(r)] \quad (14)$$

which was called a "Percus-Yevick-style" solvatation potential; it corresponds to the Percus- Yevick (PY) closure

$$c(r) = [h(r) + 1]\frac{f(r)}{f(r) + 1} \quad (15)$$

where $f(r) = \exp[-u(r)/k_BT] - 1$ is the Mayer function. In the present study, we use both potentials (12) and (14). For the bicomponent system "polymeric chain + particles", the function $\rho_d^{-1}\chi_{dd'}(r)$, which is the **r**-space representation of the structure factor $S_{dd'}(q)$, is obtained by solving equations (7) and (13) or (15). Substitution of $\chi_{dd'}$ into equation (8) gives c_{pd}. Having $\chi_{dd'}$ and c_{pd}, we can calculate the effective *intra*chain interaction $\Delta\Psi_{\alpha\beta}(r)$ between chain sites α and β separated by distance r.

As is seen from equation (8), the direct correlation function c_{pd} depends on the *intra*chain correlation function $w(r)$, *i.e.*, on the specific conformation of the whole chain. In other words, c_{pd} is a nonlinear functional of $w(r)$. Consequently, the effective *intra*chain potential $\Delta\Psi_{\alpha\beta}(r)$ also depends on $w(r)$. Hence, for given external parameters (ρ_d, T and so on), the potential $\Delta\Psi_{\alpha\beta}(r)$ depends not only on the argument r but on the spatial localization of all the other sites (monomers) of a chain as well. As a result, the probability of any given chain conformation in a dense medium depends on the whole *intra*chain potential, $\Psi(\mathbf{r}_1, ..., \mathbf{r}_N) = \sum_{\alpha<\beta}^{N}[u_{\alpha\beta}(r) + \Delta\Psi_{\alpha\beta}(r)]$. Introducing the notation $\Omega(\mathbf{r}_1, ..., \mathbf{r}_N)$ for the equilibrium conformation probability distribution function of a single N-site polymer chain in an external field produced by surrounding medium, we have

$$\Omega(\mathbf{r}_1, ..., \mathbf{r}_N) = Z^{-1}\exp\{-\Psi[\mathbf{r}_1, ..., \mathbf{r}_N; w(\mathbf{r}_1, ..., \mathbf{r}_N)]/k_BT\} \quad (16)$$

where Z is the normalization integral. The distribution $\Omega(\mathbf{r}_1, ..., \mathbf{r}_N)$ gives the *intra*chain distribution function averaged over all polymer conformations:

$$w(r) = \frac{1}{N}\sum_{\alpha,\beta}^{N}[\delta_{\alpha\beta}\delta(r) + (1 - \delta_{\alpha\beta}) \times \int d\mathbf{r}_1 ... d\mathbf{r}_N \delta(r - r_{\alpha\beta})\Omega(\mathbf{r}_1, ..., \mathbf{r}_N)]. \quad (17)$$

Here, $\delta(r)$ is the Dirac delta-function. Substitution of $w(r)$ from equation (17) to equation (8) permits to find the *inter*molecular pair correlation functions c_{pd} and h_{pd} (provided the corresponding density-density correlation function $\chi_{dd'}$ of pure solvent (medium) has been previously found for given conditions). Then the medium-induced interaction potential $\Delta\Psi_{\alpha\beta}$ is determined from equations (12) or (14). Finally, it is used in equations (16, 17) to calculate $w(r)$. Thus, we obtain the self-consistent procedure for calculation of chain equilibrium conformation in the external field, and this field itself depends on the specific equilibrium conformation of the chain. From another viewpoint, this procedure can be regarded as an algorithm for calculation of the self-consistent medium-induced site-averaged *intra*molecular potential of a flexible molecule with internal degrees of freedom

$$\Delta\Psi(r) = \frac{1}{N^2}\sum_{\alpha,\beta}^{N}\int d\mathbf{r}_1 ... d\mathbf{r}_N \Delta\Psi_{\alpha\beta}(r)\Omega(\mathbf{r}_1, ..., \mathbf{r}_N). \quad (18)$$

As can be seen from equations (17, 18), calculation of the equilibrium functions $w(r)$ and $\Delta\Psi(r)$ implies calculation (or estimation) of $3N$-dimensional integrals. In the present article, this is made *via* Monte-Carlo simulation.

Suppose that the bare potentials $u_{dd}(r)$, $u_{pd}(r)$, and $u_{pp}(r)$ describing the interactions between colloidal particles and polymeric units are specified and the density of particles ρ_d and temperature T are given. Let us also suppose that the chain model and the method of generation of chain conformations are chosen. Then the self-consistent MC/RISM scheme should consist of the following steps:

Step 0

(a) An initial chain configuration, $\{\mathbf{r}\} \equiv \{\mathbf{r}_1, ..., \mathbf{r}_N\}$, is obtained.
(b) Using one of the closure equations (Eqs. (13) or (15)), the OZ equation (Eq. (7)) is solved for the medium particles; this gives the correlation function $\chi_{dd'}$.
(c) Potential $\Delta\Psi_{\alpha\beta}(r)$ is set equal to zero.
(d) The iteration counter s is set to $s = 0$.

Step 1

(a) The set of k chain configurations is generated by MC method. The "move" $\{\mathbf{r}\} \to \{\mathbf{r}'\}$ is accepted according to the standard Metropolis criterion with the transition probability

$$\mathcal{P} = \min\left\{1, \exp\left[\frac{\Psi(\{\mathbf{r}\}) - \Psi(\{\mathbf{r}'\})}{k_BT}\right]\right\} \quad (19)$$

where

$$\Psi(\{\mathbf{r}\}) = \sum_{\alpha<\beta}^{N}[u_{pp}(r_{\alpha\beta}) + \Delta\Psi(r_{\alpha\beta})]. \quad (20)$$

(b) For the latest kth configuration $\{\mathbf{r}\}_k$ obtained as a result of "Step 1a", the *intra*chain correlation function $w_k(r)$ is evaluated.
(c) The m-time repetition of the points (a) and (b) provides data for an intermediate averaged function

$$w_m(r) = m^{-1}\sum_{k}^{m} w_k(r) \quad (21)$$

and its Fourier transform $\hat{w}_m(q)$.

Step 2

(a) The function $\hat{w}_m(q)$ is used in the Fourier **q**-space representation of equation (8),

$$\rho_d \hat{h}_{pd}(q) = \hat{w}_m(q)\hat{c}_{pd}(q)\hat{\chi}_{dd'}(q). \quad (22)$$

Using closure approximations (13) or (15) relating the c_{pd} to h_{pd} and u_{dp}, we obtain the correlation functions $\hat{c}_{pd}(q)$ and $\hat{h}_{pd}(q)$ from equation (22).

(b) Substitution of $\hat{c}_{pd}(q)$ and $\hat{\chi}_{dd'}(q)$ into equations (12) or (14) provides the evaluation of the effective potential (averaged over all N chain units) in the **q**-space

$$\Delta\Psi_m(q) = -k_B T \hat{c}_{pd}(q)\hat{\chi}_{dd'}(q)\hat{c}_{d'p}(q) \quad (23)$$

or

$$\Delta\Psi_m(q) = -k_B T \ln[1 + \hat{c}_{pd}(q)\hat{\chi}_{dd'}(q)\hat{c}_{d'p}(q)]. \quad (24)$$

(c) The function $\Delta\Psi_m(q)$ is transformed to $\Delta\Psi_m(r)$.

Step 3

(a) The iteration counter s is increased by unity: $s = s+1$.

(b) The current mean value of the effective potential is calculated

$$\Delta\Psi_s(r) = s^{-1}\sum_{m}^{s} \Delta\Psi_m(r). \quad (25)$$

(c) The potential $\Delta\Psi(r)$ in equation (20) is replaced by the new one: $\Delta\Psi(r) = \Delta\Psi_s(r)$.

(d) The convergence of the iteration procedure is examined together with the achievement of the accuracy needed for the evaluated characteristics. The calculations returns to "Step 1" if the certain accuracy is not obtained.

In accordance with the objectives of the present study stated above we consider here the simplest athermal model of a bicomponent system. We consider colloidal particles as mutually impenetrable hard spheres of diameter σ_d; n_d such particles are placed in volume V, so that the number density is $\rho_d = V/n_d$ and the volume fraction of particles is $\Phi = \pi\sigma_d^3\rho_d/6$. Similarly the polymeric units are regarded as hard spheres (beads) of diameter σ_p. This implies that we restrict interactions in our system to the simplest hard-core potential

$$u_{ij}(r) = \begin{cases} \infty, & \text{if } r < \sigma_{ij} \\ 0, & \text{if } r \geq \sigma_{ij} \end{cases} \quad (26)$$

where $\sigma_{ij} = (\sigma_i + \sigma_j)/2$, and r is the distance between the corresponding interacting sites i and j (i, $j = d$ or p).

We use a simple model of a flexible linear macromolecule with excluded volume interaction. This model (usually called bead or pearl-necklace model) is standard in polymer physics (see for example, Refs. [40,41]). The chain consists of N identical hard-sphere beads with a diameter σ_p. Their centers are connected in a chain-like manner by the volumeless "threads", *i.e.*, bonds. The bond length b is not strongly fixed and may fluctuate in some range $(1 \pm \Delta)b$ with the average being approximately equal to the prescribed value of b (Δ is the bond gap). In this aspect, the model resembles the well-known lattice *bond fluctuation model*, but, not being constricted to any lattice, it permits continuous motions for chain units. That is why we call it the continuum bond fluctuation model (CBFM). The average bond length $\langle b \rangle$ is determined by an appropriate choice of the parameters b and Δ. In the present study we accepted $b = 5\sigma_p/2$ and $\Delta = 3\sigma_p/2$ since this provides sufficient displacement of the chain beads. It should be noted that these values of b and Δ do not prevent self-intersection of the chain. However, as was noted above, if the mean distance between beads is large enough this diminishes deviations from the pairwise additivity in the N-site medium-induced potential $\Delta\Psi$. This choice of the parameters also provides very quick conformational relaxation of a chain. The corresponding model will be called "Model 1". This model is implied everywhere if the opposite is not explicitly indicated. Figure 1 gives a schematic representation of the model. Besides, in order to mimic a tangent hard-sphere chain model, we consider the bond fluctuation chains with $b = \sigma_p$. This value of b allows bonded beads to inter-penetrate by an amount equal to the bond extension Δ but does not practically allow bond crossing. This model will be called "Model 2". In addition, calculations for the chains with some other bond lengths were carried out. For all the models, the bead diameter σ_p was set to 0.2. At $\sigma_p = 0$ and $\rho_d = 0$, the chains behave ideally and obey Gaussian or random-walk statistics. For a Gaussian chain, the mean end-to-end distance behaves as $\langle R^2(N) \rangle = \langle (\mathbf{r}_1 - \mathbf{r}_N)^2 \rangle = \langle b^2 \rangle (N-1)$.

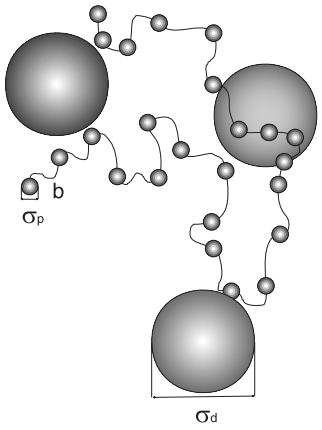

Fig. 1. Schematic representation of the system "polymer chain + colloidal particles" and the continuous bond-fluctuation model (CBFM) of a polymer chain.

An initial chain conformation is generated as a self-avoiding random walk. Starting from the initial conformation, we randomly pick bead α with the position vector $\mathbf{r}_\alpha$ and try to move this bead in a randomly chosen

direction $\mathbf{r}'_\alpha = \mathbf{r}_\alpha + \delta$, where $0 \leq |\delta| \leq 0.2$. The trial position $\mathbf{r}'_\alpha$ in the Monte-Carlo algorithm is accepted only if neither the restriction on the allowed range of the bond length nor the excluded volume constraint are violated. Of course, it is straightforward to include effects due to an *intra*chain medium-induced interaction energy into this algorithm (see Eq. (19)). All the beads of our chain (excluding the adjacent ones) interact in a pairwise way *via* the $\Delta\Psi$ potential. Time t is measured in Monte-Carlo steps per bead. One MC step (MCS) means that on average each chain bead has attempted to move once, successfully or unsuccessfully. For the isolated chains with excluded-volume interactions between elements of the chain, the mean size of the chain R grows as N^ν, where $\nu \approx 0.6$, in agreement with polymer theories [10,40,41].

The RISM equations were solved using the modified Picard iteration scheme [42], but the variational and mixed Newton-Raphson techniques are possible as well. The method of fast Fourier transformation (FFT) was used for calculation. The number of integration points was $L = 2^{10} \div 2^{12}$, both in the r and q variables. The step size $\Delta r = R_c/L$ was 0.05 or 0.025. Note that R_c must be $R_c > \langle b \rangle (N-1)$. The integral equations were solved for $\hat{\gamma}(q) = \hat{h}(q) - \hat{c}(q)$. The iterations are performed until the self-consistency condition

$$|1 - \gamma^{out}(r)/\gamma^{in}(r)| < 10^{-6} \tag{27}$$

is satisfied.

For an ideal N-unit chain (random walk) a longest relaxation time (Rouse time) scales as $\tau_N \propto N^2$ [10,41]. In the MC simulation, τ_N is the number of attempted moves. Following this estimate we set $k = N^2$ for "Step 1a". As for the value of m in equation (21), this number is chosen to be $m = 1000$ for all N considered. Thus, the total number of MC moves for one of the self-consistent iteration was $km = 1000N^2$ for each chain length and density ρ_d. The $\hat{w}(q)$ was averaged over these configurations and then used in the RISM theory to obtain the *inter*molecular correlations and a new medium-induced potential.

In the course of calculations, the functions $w(r)$ and $\Delta\Psi(r)$ were monitored. After the completion of each sth iteration, the change of the effective potential $\Delta\Psi(r)$ and the effective monomeric second virial coefficient

$$B^* = 2\pi \int_{(r)} dr r^2 \{1 - e^{-[u_{pp}(r) + \Delta\Psi(r)/k_B T]}\} \tag{28}$$

was checked. In addition, we control the bead-bead *intra*chain energy

$$U_{pp} \equiv \Psi(\mathbf{r}_1, ..., \mathbf{r}_N) = \sum_{\alpha<\beta}^{N} [u_{pp}(r_{\alpha\beta}) + \Delta\Psi(r_{\alpha\beta})]. \tag{29}$$

In the general case, both B^* and U_{pp} depend on the number of iterations, s, and are calculated as values averaged over km Monte-Carlo steps. Disappearance of systematic trends in $\Delta\Psi(r)$, B^*, and U_{pp} is the criterion of convergence of the iteration procedure. Generally this occurs after two or three iterations. Typical example of the U_{pp} behavior is shown in Figure 2 for the hard-core chains (Model 1) with $N = 32$, 64, and 96 at $\rho_d = 0.8$ ($\Phi = 0.419$) and $\gamma \equiv \sigma_d/\sigma_p = 5$. We can see that U_{pp} has quite large fluctuations at $s \leq 3$, and after this it reaches a final level, about which it fluctuates randomly. For this steady state, calculation of all the global averages was made. As a rule, the total number of iterations was $s = 100 \div 200$. Namely, for $N = 96$ the full number of MC moves was $kms = 1.8 \times 10^9$.

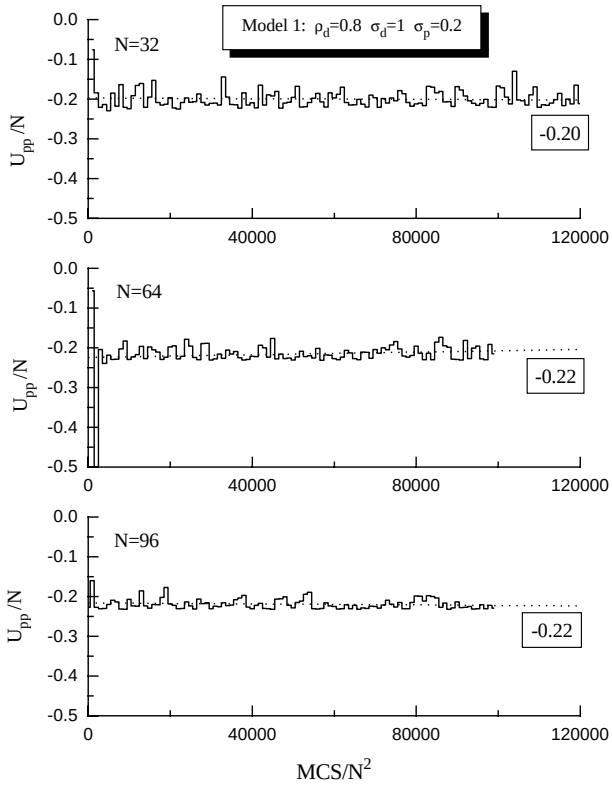

Fig. 2. Time evolution of the *intra*chain effective energy per monomeric unit for three different values of N at particle density $\rho_d = 0.8$ and size ratio $\gamma = 5$. The time-averaged values of $\langle U_{pp} \rangle / N$ are presented near the curves. The data are obtained by the MC/RISM method with the HNC-type potential for the Model 1.

3 Results of calculations

3.1 Dependence on the density of particles

Let us define the so-called expansion factor of a polymeric coil

$$\alpha^2 = \frac{\langle R^2(N, \rho_d) \rangle}{\langle R^2(N, 0)_\Theta \rangle} \tag{30}$$

where the index Θ indicates the absence of excluded volume interaction ($\sigma_p = 0$). Note that the value of α^2 is one of the main characteristics of the coil. In Figure 3 we present α^2 as a function of the volume fraction of colloidal

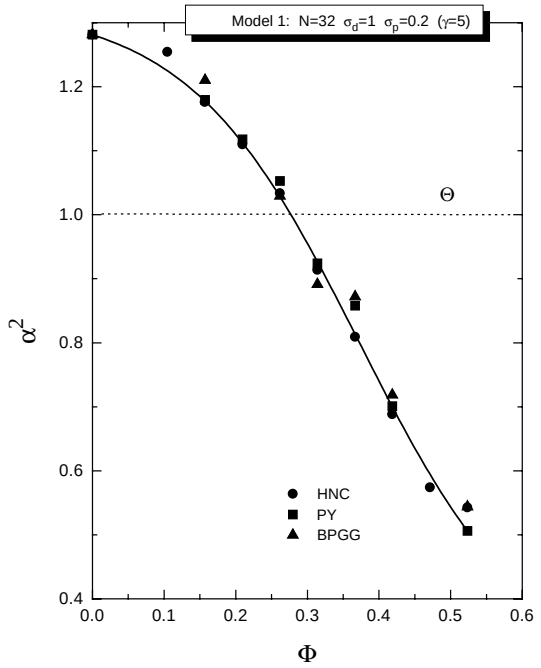

Fig. 3. α^2 *vs.* particle packing fraction Φ for CBFM polymer chain with $N = 32$ monomeric units at size ratio $\gamma = 5$. The data are obtained by the MC/RISM method for the Model 1, using the HNC closure (Eq. (13)) and the HNC-type effective potential (Eq. (12)) as well as the PY closure (Eq. (15)) and the PY-type effective potential (Eq. (14)). In addition, the results corresponding to the Ballone-Pastore-Galli-Gazillo (BPGG) closure relation (Eq. (31)) and the HNC-type potential (Eq. (12)) are presented.

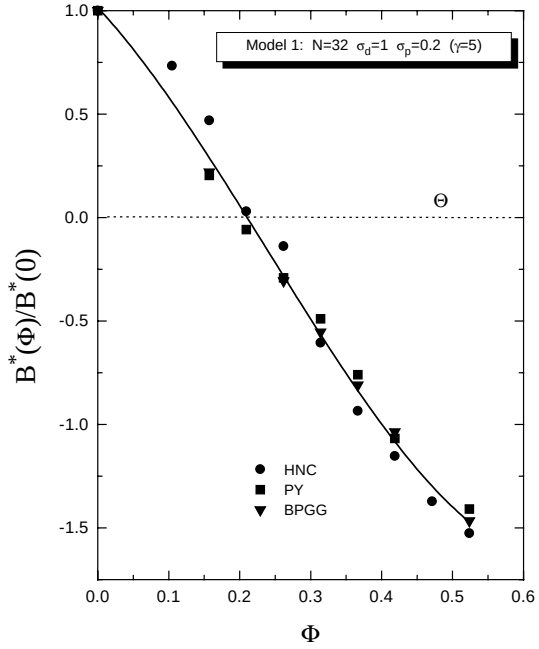

Fig. 4. The normalized effective monomeric second virial coefficient $B^*(\Phi)/B^*(0)$ *vs.* Φ for $N = 32$ and $\gamma = 5$. The data are obtained by the MC/RISM method for the Model 1, using the HNC closure (Eq. (13)) and the HNC-type effective potential (Eq. (12)) as well as the PY closure (Eq. (15)) and the PY-type effective potential (Eq. (14)). In addition, the results corresponding to the Ballone-Pastore-Galli-Gazillo (BPGG) closure relation (Eq. (31)) and the HNC-type potential (Eq. (12)) are presented.

particles, $\Phi = \pi\sigma_d^3\rho_d/6$, for the 32-unit chains; the ratio of the hard-core diameters of particles and chain beads, $\gamma = \sigma_d/\sigma_p$, is chosen to be $\gamma = 5$. The data shown in Figure 3 were obtained for the Model 1, using the HNC closure (Eq. (13)) and the HNC-type effective potential (Eq. (12)) as well as the PY closure (Eq. (15)) and the PY-type effective potential (Eq. (14)). In addition, in Figure 3 we present the results corresponding to the Ballone-Pastore-Galli-Gazillo (BPGG) closure relation [43]

$$\begin{aligned} c(r) &= h(r) - \ln[h(r)+1] + [\frac{15}{8}y(r)+1]^{8/15} \\ &\quad - y(r) + 1 - u(r)/k_BT, \\ y(r) &= h(r) - c(r) \end{aligned} \tag{31}$$

and the HNC-type potential. The values of α^2 are seen to drop in all cases. Qualitatively similar results were obtained for other hard-core chains with $N = 64$ and 96. The HNC, PY, and BPGG results coincide within the simulation statistical errors ($\approx 5\%$), and go through $\alpha^2 = 1$ at $\Phi \approx 0.27$ when the chain behaves like an ideal (unperturbed) Gaussian chain. At this particular density of colloidal particles, the medium-induced intrachain attraction effectively compensates the intrachain excluded volume interaction. The further growth in Φ leads to a diminishing of the mean chain size, *i.e.*, to a compression of the polymeric coil.

Thus, we observe that the hard-sphere medium can produces an effective attraction between polymeric units, which themselves are of the hard-core nature. This medium-induced attraction may be the physical origin of the key results of our calculations.

The appropriate measure of the medium-induced intrachain interaction is the effective monomeric second virial coefficient B^* given by equation (28). The value of B^* as a function of Φ is shown in Figure 4. Again, we do not find significant distinctions between the HNC, PY, and BPGG predictions. Traditionally, B^* is considered in polymer physics as a measure of solvent quality. The case $B^* > 0$ corresponds to a good solvent, in which the polymer swells; that is, $\alpha^2 > 1$. At $B^* < 0$, the polymer is generally collapsed, indicating a poor solvent. The case of $B^* = 0$ corresponds to a *theta* (Θ) solvent, in which the polymer is ideal, *i.e.*, $\alpha^2 = 1$. Figure 4 shows that B^* decreases with Φ and crosses the Θ line at $\Phi \approx 0.21$; then it becomes increasingly negative. In terms of the physics of polymer solutions, this means that upon increasing density the hard-core medium becomes a poor solvent for a polymer. However, comparison of Figures 3 and 4 shows that for relatively short chains considered here the equalities $\alpha^2 = 1$ and $B^* = 0$ turn true at slightly different Φ.

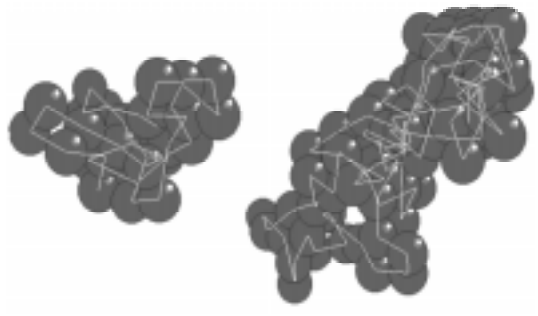

Fig. 5. A projection in the xy plane of the configurations ("snapshots") of 32 and 96-unit chains after $s = 100$ MC/RISM iterations at $\rho_d = 0.8$ and $\gamma = 5$. The calculations are performed for the Model 1.

The functions $\alpha^2(\Phi)$ and $B^*(\Phi)$ exhibit similarity: both appear to be S-like curves.

Thus, the hybrid MC/RISM approach predicts the compression of a polymeric coil immersed in the athermal medium with increasing density of medium. It should be emphasized here that, in our hard-core system, the only incentive for such a behavior is the effective medium-induced interaction between chain units. If density ρ_d is high enough, we observe the polymer *collapse* for the Model 1, *i.e.*, the transition to the globular state. In general, the same features were observed in the case of the lattice MC many-particle simulations [12–14]. In Figure 5 we present some typical examples of the globular configurations obtained for the Model 1 with $N = 32$ and $N = 96$ at $\rho_d = 0.8$ ($\Phi = 0.419$).

Now let us consider the results obtained for the Model 2 (which seems to be a more representative model of a realistic polymer chain). Figures 6 and 7 show the corresponding values of α^2 and B^* *versus* packing fraction Φ, calculated for $N = 32$ and the size ratio $\gamma = 2.5$ with the HNC closure and the HNC-type solvation potential. Using the PY-type potential gives very similar results. One can see that, although a sufficiently strong contraction of the chain takes place at high particle densities (when B^* approaches zero and even becomes negative), the polymer sizes predicted by our hybrid MC/RISM method for the Model 2 do not reach the Θ size at $\gamma = 2.5$, and even more so at any other γ. Moreover, at high density, increasing chain length leads to an increase in α^2: as can be seen from Figure 8, at $\Phi = 0.556$ the value of α^2 scales with chain length as $\alpha^2 \propto N^{\delta}$, where $\delta \approx 0.2$. This behavior corresponds to the known scaling of $\langle R^2 \rangle$ with chain length, $\langle R^2 \rangle \propto N^{2\nu}$, observed for chains in a good solvent, where $\nu \approx 0.6$. This leads us to speculate that the variation with density of chain size at high colloid densities may be quite dependent on the exact local features of polymeric models. In other words, whether the hard-core polymer chains collapse or not is a delicate balance between the repulsive, intrachain excluded volume interactions and the medium-induced attraction. This observation is consistent with the predictions of the work

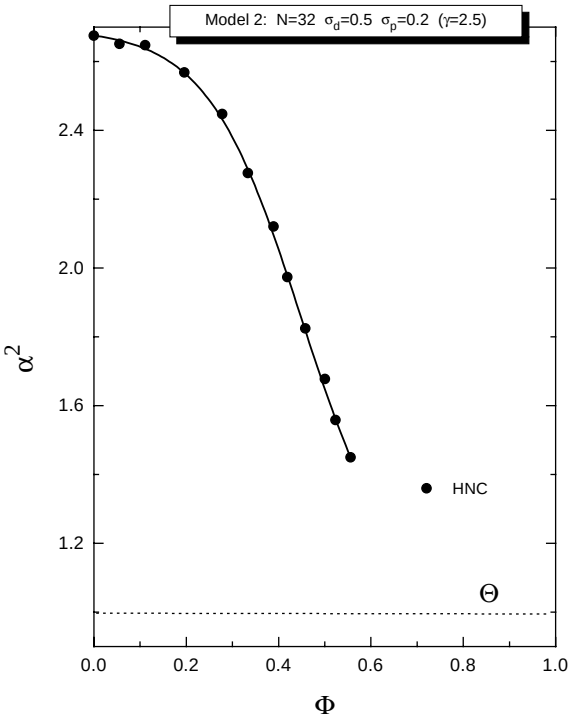

Fig. 6. α^2 as a function of Φ for $N = 32$ at $\gamma = 2.5$. The data are obtained by the MC/RISM method for the Model 2, using the HNC closure relation (Eq. (13)) and the HNC-type effective potential (Eq. (12)).

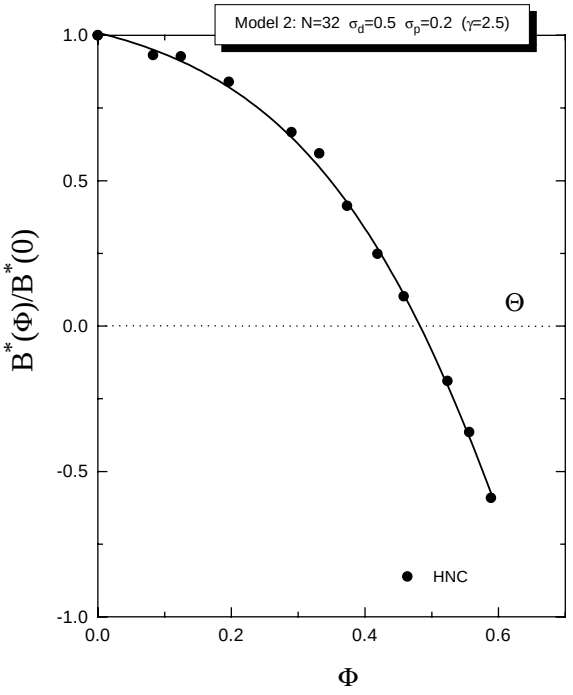

Fig. 7. The normalized effective monomeric second virial coefficient $B^*(\Phi)/B^*(0)$ as a function of Φ for $N = 32$ at $\gamma = 2.5$. The data are obtained by the MC/RISM method for the Model 2, using the HNC closure relation (Eq. (13)) and the HNC-type effective potential (Eq. (12)).

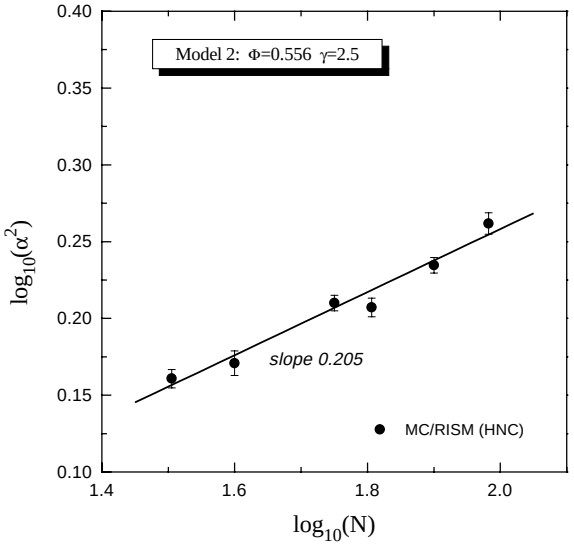

Fig. 8. $\log_{10}(\alpha^2)$ *vs.* $\log_{10}(N)$ at particle packing fraction $\Phi = 0.556$ and $\gamma = 2.5$. The data are obtained for the Model 2 using the HNC closure relation (Eq. (13)) and the HNC-type effective potential (Eq. (12)).

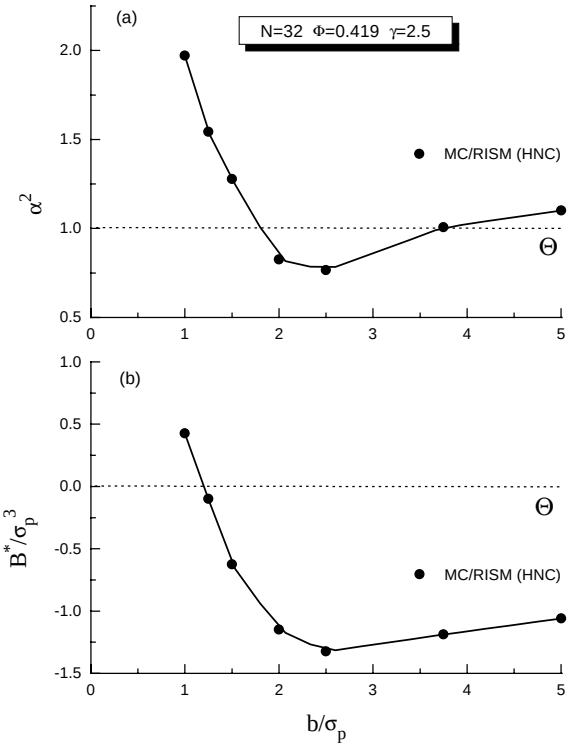

Fig. 9. α^2 and B^* as functions of bond length at particle packing fraction $\Phi = 0.419$ and $\gamma = 2.5$. The data are obtained for the HNC closure relation (Eq. (13)) and the HNC-type effective potential (Eq. (12)).

by Grayce on nonadditivity effects and many-body solvation potentials based on "scaled particle theory" (SPT) [44]. As has been shown by Grayce, there may not be athermal polymer collapse in hard-sphere solvents, at least for the chain models considered in this work.

Below we present some additional results obtained by the self-consistent MC/RISM method for the chains with various bond length.

3.2 Dependence on the bond length

Figure 9 shows α^2 and B^* for a hard-core 32-mer as functions of bond length b, calculeted using the HNC closure relation and the corresponding solvation potential at $\Phi = 0.419$ and $\gamma = 2.5$. We find that in the region $b < 2.5\sigma_p$ the value of α^2 decreases gradually as b is increased and then begins to grow. At $b \approx 1.75\sigma_p$ and $b \approx 3.75\sigma_p$, α^2 crosses the Θ line, where $\alpha^2 = 1$. The effective monomeric second virial coefficient becomes negative at $b \geq 1.2\sigma_p$ and appears to be a slowly increasing function of bond length at $b > 2.5\sigma_p$. Thus, we conclude that, in the athermal polymer/colloid system, the hard-core chains may exhibit a nonuniversal behavior, depending on the bond length which determines the intrachain excluded volume interactions in the model under consideration. In the region $1.75 < b/\sigma_p < 3.75$, the chain collapses; beyond this region, the polymeric coil remains in a swollen state. Below our calculations focus mainly on $b = 2.5\sigma_p$, *i.e.*, on the value of b corresponding to the Model 1.

3.3 Dependence on the particle size

Let us keep the volume fraction Φ of colloidal particles fixed and analyze the influence of particle size at $\sigma_p = constant$. All the data presented in this subsection were calculated for a rather dense medium ($\Phi = 0.419$). Clearly, at $\sigma_d = 0$ we deal with an isolated chain with excluded volume interaction; the latter is determined by the hard-core diameter of a monomeric unit σ_p. Figures 10 and 11 present α^2 and B^* as functions of parameter $\gamma = \sigma_d/\sigma_p$, calculated for the Models 1 and 2. The main body of the calculations is performed for the HNC approximation, however, the comparison with data based on the PY and BPGG approximations shows practical coincidence of the results within the simulation statistical errors (see Fig. 10a). It is seen from Figure 10 that the reduction of mean chain dimensions takes place already at rather small values of γ. In the case of the Model 1, polymer chain attains Θ dimensions with increasing γ; further growth of γ leads to the coil-globule transition at $\gamma \approx 3$. After that an opposite process takes place. Thus, we observe the nonmonotonic dependence of mean chain dimensions. The B^* function manifests similar behavior (Fig. 11). For the Model 2, the function $\alpha^2(\gamma)$ is also nonmonotonic. However, in this case we do not observe the chain collapse at any γ (Fig. 10b).

Also, we can consider the chain size as a function of the mean interparticle distance, which is estimated

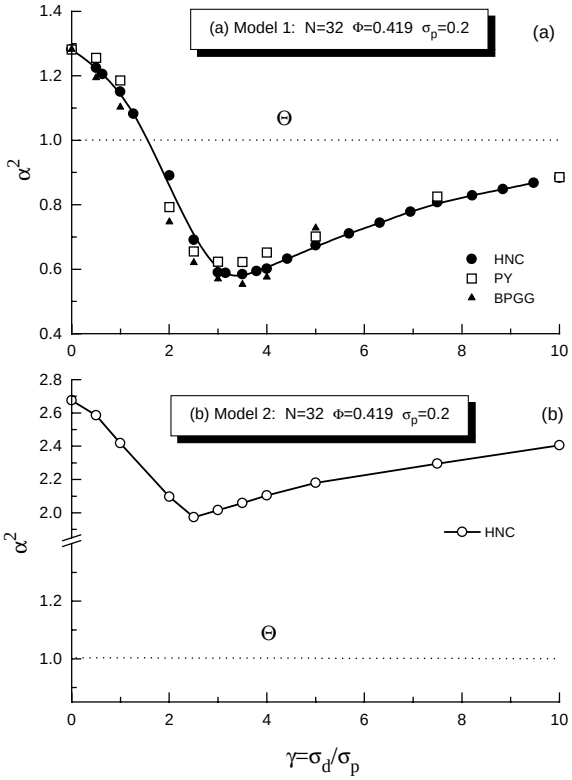

Fig. 10. (a) α^2 *vs.* γ for $N = 32$ and $\Phi = 0.419$. The cycles are the result of the MC/RISM method using the HNC closure and the HNC-type potential. The squares indicate the results obtained by the MC/RISM method with the PY closure and the PY-type potential. The triangles are the result of the MC/RISM method for the BPGG closure relation and the HNC-type potential. The data are obtained for the Model 1. Notice the minimum near $\gamma = 3$. (b) α^2 *vs.* γ for $N = 32$ and $\Phi = 0.419$. The data are obtained for the Model 2, using the HNC closure and the HNC-type potential.

as $2\pi/q_{max}$, where q_{max} denotes the position of the first peak of the structure factor

$$S_{dd'}(q) = 1 + \rho_d \hat{h}_{dd'}(q). \tag{32}$$

Figure 12 presents these data obtained for the Model 1. It is seen that the plots α^2 *vs.* γ (Fig. 10a) and $\langle R^2 \rangle$ *vs.* $2\pi/q_{max}$ (Fig. 12) are similar because $q_{max}^{-1} \sim \sigma_d$ (see the insert in Fig. 12).

Clearly, in the $\gamma \to 0$ case we have a continuous structureless medium which does not affect the correlation functions of embedded larger objects (*i.e.*, polymeric units with finite size). Therefore, all the chain properties are determined solely by the bare potential. On the other hand, the opposite case, when $\gamma \to \infty$, corresponds to a single chain trapped between impenetrable obstacles randomly distributed in three-dimensional space (at $\Phi < 1$). In this system, there are holes (or empty volume) with characteristic size $\sim (2\pi/q_{max} - \sigma_d)$, which is sufficient for any finite N-unit chain to be trapped as a whole in one of these holes (because at any N the volume of polymeric coil $V_N \sim N^{3\nu}$ is smaller than the volume of a hole $\sim (2\pi/q_{max} - \sigma_d)^3$).

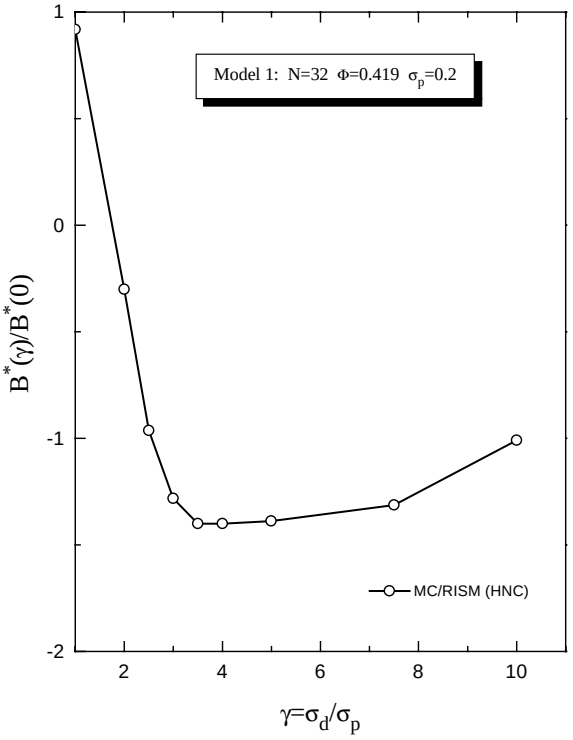

Fig. 11. Plot of the normalized effective monomeric second virial coefficient $B^*(\gamma)/B^*(0)$ as a function of γ for $N = 32$ and $\Phi = 0.419$. The error bars indicate the standard deviation of the mean values. The calculations are performed for the Model 1 using the HNC-type potential.

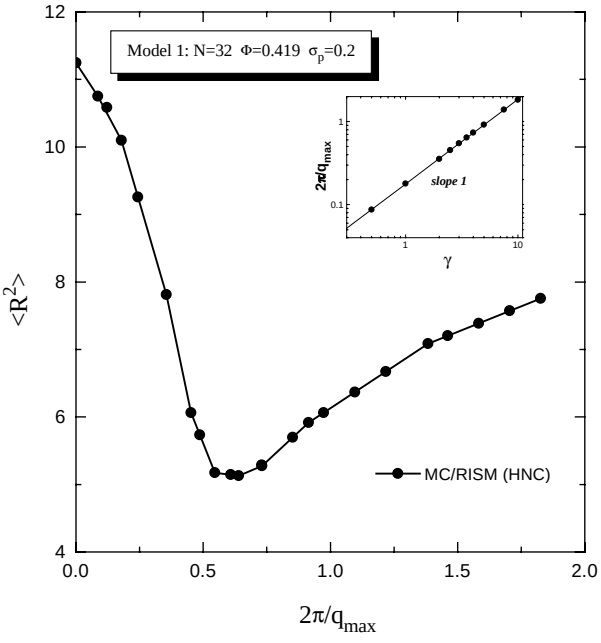

Fig. 12. $\langle R^2 \rangle$ *vs.* $2\pi/q_{max}$ for $N = 32$ and $\Phi = 0.419$. Insert: $2\pi/q_{max}$ *vs.* γ. The calculations are performed for the Model 1 using the HNC-type potential.

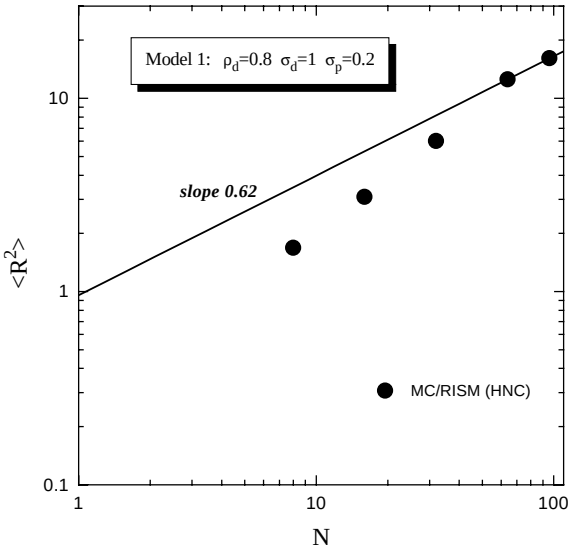

Fig. 13. $\langle R^2 \rangle$ *vs.* N on a double logarithmic scale for $\rho_d = 0.8$ and $\gamma = 5$. The calculations are performed for the Model 1 using the HNC-type potential.

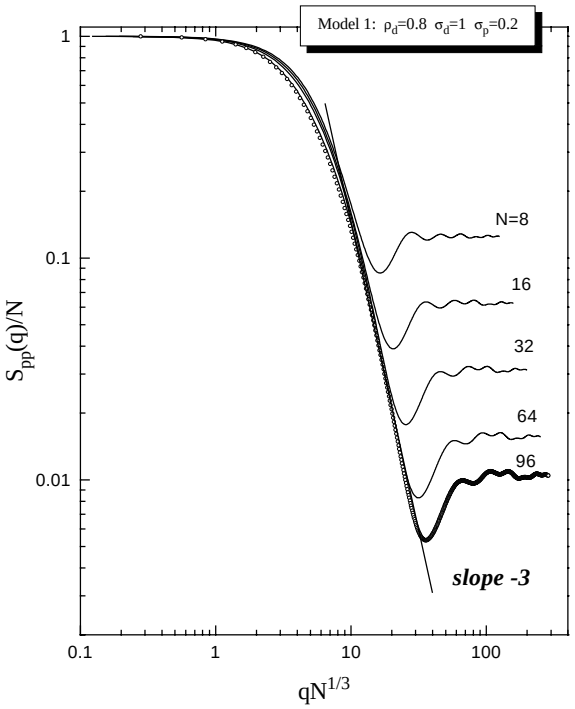

Fig. 14. The average *intra*chain static structure factor, $S_{pp}(q)/N$, *versus* $\sigma_d q N^{\nu}$, where $\nu = 1/3$. The curves represent the results for five different values of N (see right-side part of the figure); $\rho_d = 0.8$ and $\gamma = 5$. For intermediate q, the effective, medium-induced, *intra*chain interaction causes the scattering function to behave like $S_{pp}(q) \propto q^{-1/\nu}$ that corresponds to the globular state of polymer chains. It is seen that for $\sigma_d q \lesssim 10 N^{\nu}$ the curves coincide. The insensitivity to N indicates that even ~ 10 beads is near the scaling limit in this q region. For larger q, the chain beads are uncorrelated and $S_{pp}(q) \to 1/N$. At $q \to 0$, $S_{pp}(q) \to N$. The calculations are performed for the Model 1 using the HNC-type potential.

Again, the properties of the chain are obviously determined solely by the bare potential, so we can expect that the mean size of the polymer is the same as of an isolated chain. Although we have not made calculations for this case, the respective tendency in α^2 or $\langle R^2 \rangle$ is distinctly seen in Figures 10 and 12. Similar features are observed for B^*. As a result, we have the curves with the minimum, *i.e.*, nonmonotonic dependencies on γ. At $\gamma \gtrsim 1$ and $\Phi < 1$, there are holes of sufficiently large size. Since from the point of view of conformational entropy the position of a chain in these regions is favorable, these regions can be regarded as "entropic traps" or "entropic potential wells". Thus, it is natural to expect that due to the presence of such traps the chain will adopt the conformation that is more compact than the conformation in an infinite empty volume. Our analysis shows that this indeed the case. The real question is what is the degree of this shrinking and whether the chain conformation becomes globular. Of course, the capacity of each entropic trap to adsorb chain links is finite. Therefore, due to the excluded volume of the links the variation of chain conformation may not be solely a reflection of the change in medium density and particle size, but rather a result of changes in the local properties of polymeric models (bead size, chain rigidity, bond length, *etc.*) which determine the effective intrachain excluded volume.

3.4 Dependence on the chain length and size scaling

The simplest ("customary") way of demonstrating the scaling behavior of polymers is to plot the mean-square size vs. the number of units in the polymer chain. Such a plot is shown in Figure 13 for polymers (with $N = 8 \div 96$) surrounded by particles at $\gamma = 5$ and $\rho_d = 0.8$. The mean size $R \equiv \langle R^2 \rangle^{1/2}$ of a polymer globule scales with N as $R \propto N^{1/3}$ at $N \gg 1$. Because we studied only a few chains of finite length, it is very difficult to extract a convincing result for the N dependence from our data; a more extensive calculation involving much larger chains would be useful. Nevertheless, in Figure 13 we see the trend in data to approach the expected power law $R^2 \propto N^{2/3}$ for $N > 32$.

A more detailed scaling analysis of computer results can be made by using the static structure factor $S_{pp}(q)$ of polymer chains. Clearly, in an infinitely dilute system "chain + particles" the function $S_{pp}(q)$ is certainly nothing but the averaged intramolecular correlation function $\hat{w}(q)$. The corresponding scaling plot of $S_{pp}(q)/N$ *vs.* $qN^{1/3}$ is presented in Figure 14 for various N. We find excellent agreement with the expected behavior: it is seen that there is a universal behavior for $1/q$ larger than a mean bond distance; at large $1/q$ all the curves coincide.

Thus we conclude that, at high density of medium consisting of hard-sphere particles, a flexible chain forms a globule. If the chain length is large enough the compact globule appears, which exhibits a number of universal

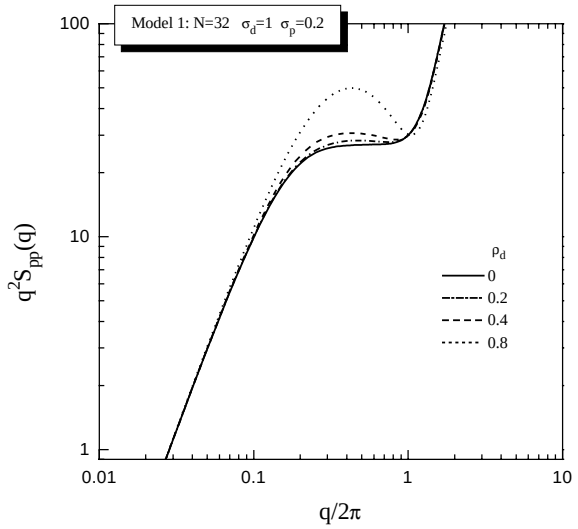

Fig. 15. Average *intra*chain static structure factor of a hard-core chain of length $N = 32$ at $\gamma = 5$ and various ρ_d, plotted in standard Kratky form. The calculations are performed for the Model 1 using the HNC-type potential.

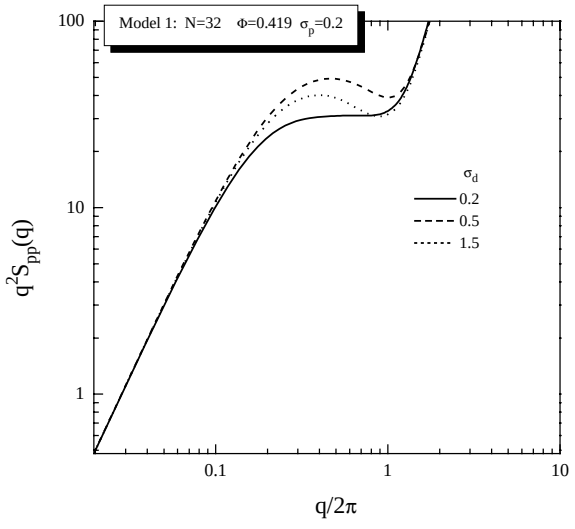

Fig. 16. Average *intra*chain static structure factor of a hard-core chain of length $N = 32$ at $\Phi = 0.419$ and various γ ($\gamma = 1$, 2.5, and 7.5), plotted in standard Kratky form. The calculations are performed for the Model 1 using the HNC-type potential.

features. In addition to the size scaling, it is possible to observe constant value of the effective *intra*chain energy per monomer unit (see Fig. 2).

The following two subsections present more details concerning the globular structure.

3.5 Chain structure

Figures 15 and 16 show some typical medium-density and particle-size results for the average *intra*chain correlation function $S_{pp}(q)$ of a hard-core chain of length $N = 32$, plotted in the standard Kratky form. As is seen from Figure 15, at $\gamma = constant$ the appreciable changes of the chain structure as a function of particles density occur at $\rho_d \gtrsim 0.4$, which corresponds to the initial stage of rapid shrinking of a polymer coil (see Fig. 3). The characteristic scale of the structural changes, $2\pi/q\sigma_p$, corresponds to five and more monomers. From Figure 16 we can see that, at fixed volume fraction $\Phi(= 0.419)$, structural changes initiated by increasing of the particle size have the same characteristic scale as in the previous case. The influence of the medium on chain conformation is appreciable even for rather small colloidal particles comparable in size to polymer units.

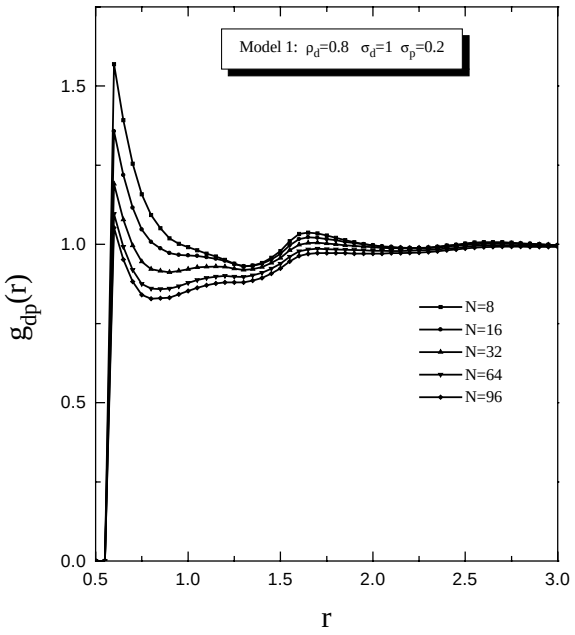

Fig. 17. Particle-polymer pair correlation function $g_{dp}(r)$ calculated by the MC/RISM method for $\rho_d = 0.8$ and $\gamma = 5$ at various N as indicated. The results are obtained for the Model 1.

3.6 Distribution of colloidal particles around chain

The distribution of colloidal particles around chain beads is described by the pair correlation function $g_{dp}(r) = h_{dp}(r) + 1$. Figure 17 presents this function for different N at $\rho_d = 0.8$. Note that at $\rho_d = 0.8$ the polymer coil is strongly compressed as compared to the isolated chain. Figure 17 shows that the function $g_{dp}(r)$ has a high fist peak in the case of short chains. This means that the globule formed by relatively short chains has friable structure. When N increases, the first peak of the function $g_{dp}(r)$ drops. Hence, the globule becomes more dense. At $N \geq 64$, the difference in distribution of particles around monomers practically vanishes.

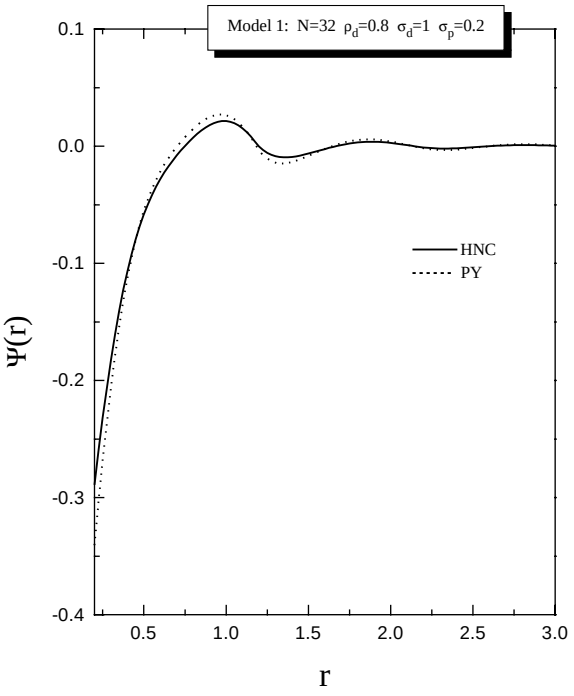

Fig. 18. The *intra*chain medium-induced potential of mean force for $N = 32$, $\rho_d = 0.8$, and $\gamma = 5$: (——) HNC theory for colloidal particles and effective *intra*chain potential, (----) PY theory for colloidal particles and effective *intra*chain potential. Note: the vertical axis is marked in units of k_BT. The results are obtained for the Model 1.

3.7 Medium-induced potential

As it is indicated above, the results obtained for mean chain dimensions practically do not depend on whether we use the HNC-type potential (Eq. (12)) or the PY-type potential (Eq. (14)). The data shown in Figure 18 confirm this. Note that for the bare hard-sphere potential used here the medium-induced potential $\Delta\Psi$ coincides with the full potential of mean force Ψ in the range $r > \sigma_p$. As it can be seen from Figure 18, there is only a slight difference between the two potentials. Hence, below we discuss only the results for HNC-type potential.

It should be noted that medium-induced potentials between chain beads have been analyzed in several papers (see, *e.g.*, Refs. [23,26,44,45]). To test the relative accuracy of the HNC and PY solvation potentials, Grayce *et al.* [26] have considered the general trends in Ψ with density for multiple-chain systems. Comparison with existing simulation data for the change with polymer density in the mean square end-to-end distance of flexible chains shows that the HNC-type potential appears to be slightly more accurate than the PY one for the hard-core chains at low (or intermediate) densities ρ, while the PY-type potential is generally more accurate for the system of Lennard-Jones (LJ) chains. Static properties of flexible LJ chains surrounded by LJ solvent particles with purely repulsive interactions between the particles and chain beads have been studied using the self-consistent MC/RISM approach and direct molecular dynamics (MD) simulations [45]. It was found that at relatively low solvent densities ($\rho_s \lesssim 0.4$) the self-consistent MC/RISM results obtained with the HNC approximation are almost identical to those obtained with the PY approximation. In this case, the differences between MC/RISM predictions and data from the many-particle MD simulations are also almost indistinguishable within the simulation statistical errors. However, it should be born in mind that, since at low (intermediate) densities the effective potentials are weak relative to the thermal energy, the two potentials are insufficiently different to produce markedly different results. Indeed, at $\rho \ll 1$ (when $\Psi \ll k_BT$) the HNC and PY potentials become equivalent by construction [23]. On the other hand, at high density the two potentials may be, in principle, quite different. For model polymer liquids, the HNC potential can lead to a pronounced contraction of the polymer chain at high densities, something not observed in real experiments [26]. Use of the PY solvation potential for polymer liquids predicts a mean chain size that becomes nearly independent of polymer density or can become slightly larger at high ρ [26]. These facts show that, in the case of one-component dense polymer liquids, the HNC-type potential is less accurate than its PY-type counterpart. On the other hand, as has been shown in reference [45] for repulsive LJ chains in monomeric solvent, the HNC approximation yields slightly more accurate predictions at $\rho_s \geq 0.5$. Overall, the intrachain correlation functions predicted by the MC/RISM method with the HNC-type potential in a wide range of solvent densities are in very good agreement with simulated data, that is the molecular structure of the polymer chains surrounded by monomeric LJ solvent is captured almost quantitatively. In the case of hard-sphere polymer/colloid systems with large size ratio γ, the problem concerning the accuracy of solvation potentials is less clear. It would be very instructive to perform the corresponding many-particles, off-lattice simulations to compare the simulated results with the theoretical predictions. At present we believe that the results obtained for our systems using the two different potentials coincide within the statistical errors ($\approx 5\%$).

The functions $\Psi(r)$ are presented in Figure 19 for various ρ_d at $\gamma = constant$. It is clear that $\Psi(r) = 0$ for all $r > \sigma_p$ when $\rho_d = 0$. At $\rho_d > 0$, the effective attraction arises in the range $r \lesssim 3\sigma_p$. When ρ_d grows, the attraction in this range increases, while at greater r the potential exhibits a long-range oscillatory behavior. Hence, the polymer shrinkage induced by the increasing medium density is due to the enhanced attraction of monomers at the *short* distances and the expansion of the attraction radius of $\Psi(r)$. For relatively short chains considered here, the medium-induced potential has a range comparable to the size of the chain. However, due to the screening effect the $\Delta\Psi$ function *does not* depend on N for sufficiently long chains (see below).

There is peculiarity in the effective potential calculated for various diameters of particles at $\Phi = constant$. Figure 20 shows that with growing γ (at $\sigma_p = constant$) the depth of the attractive well situated at small r diminishes

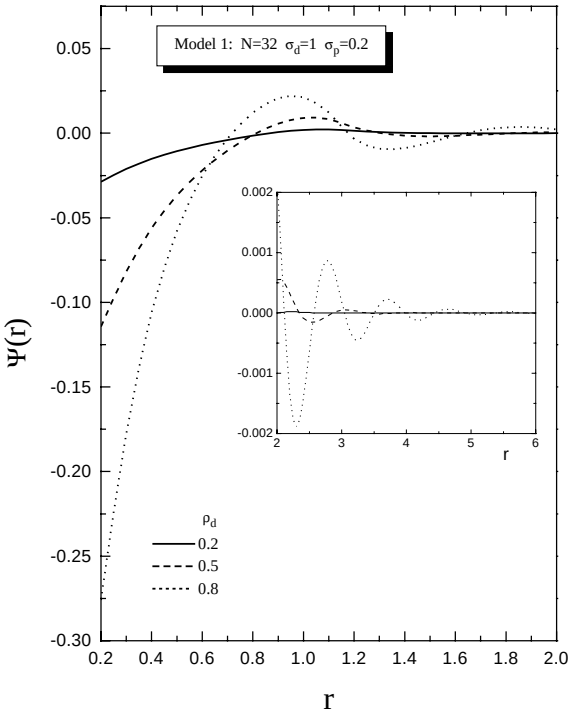

Fig. 19. The average effective *intra*chain potential of mean force between sites of a linear polymer of $N = 32$ hard-core beads of diameter $\sigma_p = 0.2$ in hard-sphere medium at $\gamma = 5$ ($\sigma_d = 1$) and various ρ_d as indicated. The data are obtained by the MC/RISM method with the HNC-type potential. Note: the vertical axis is marked in units of k_BT. The calculations are performed for the Model 1.

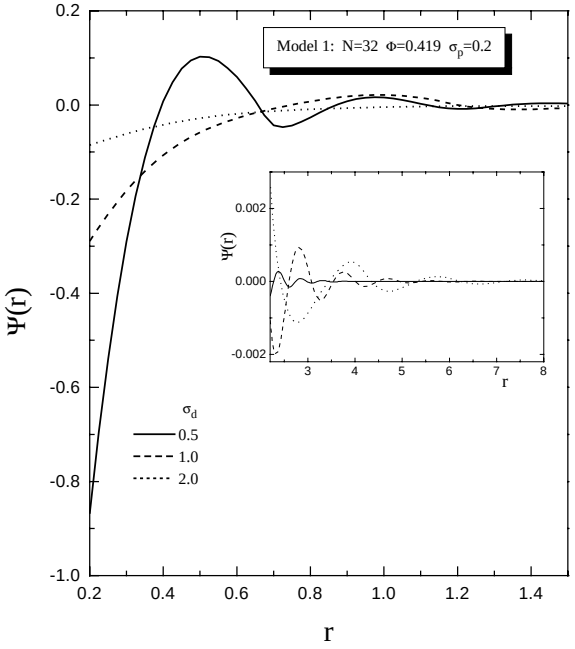

Fig. 20. The average effective *intra*chain potential of mean force between sites of a linear polymer of $N = 32$ hard-core beads of diameter $\sigma_p = 0.2$ in hard-sphere medium at $\Phi = 0.419$ and various σ_d as indicated. The data are obtained by the MC/RISM method with the HNC-type potential. Note: the vertical axis is marked in units of k_BT. The calculations are performed for the Model 1.

rapidly. At the same time, the potential $\Psi(r)$ acquires a long oscillating tail (see the insertion in Fig. 20). The period of oscillations is close to the diameter of the particle σ_d (*i.e.* these oscillations happen to be in phase with the corresponding oscillations of the particle-particle correlation function $g_{dd}(r)$).

Results obtained for $\Psi(r)$ under the same conditions at different values of N are presented in Figure 21. We see here that the effective potential reaches its final steady shape at $N \geq 32$. As we think, this result deserves a more detailed discussion in the framework of general problem concerning the application of medium-induced potentials to the reduced description of polymers. This discussion will be presented below.

4 Discussion

First of all we would like to discuss the following point: what is the physical meaning of the self-consistent medium-induced potential and is the use of such potential valid for the description of a polymer chain in dense globular (collapsed) state?

The representation of the intramolecular effective potential as a sum of the pair site(α)-site(β) components

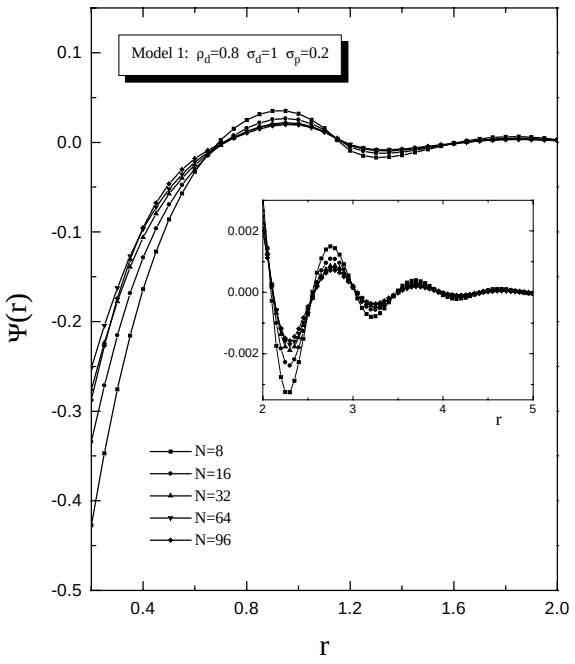

Fig. 21. The average effective *intra*chain potential of mean force between sites of a linear polymer of N hard-core beads of diameter $\sigma_p = 0.2$ in hard-sphere medium at $\gamma = 5$ ($\sigma_d = 1$) and $\rho_d = 0.8$. The data are obtained by the MC/RISM method with the HNC-type potential. Note: the vertical axis is marked in units of k_BT. The calculations are performed for the Model 1.

$\Delta\Psi_{\alpha\beta}$ depending on distances $r_{\alpha\beta} = |\mathbf{r}_\alpha - \mathbf{r}_\beta|$ (as well as on $w(r)$ and the structure of medium $\chi_{dd'}$) implies the following assumption: the magnitude of $\Delta\Psi_{\alpha\beta}$ is completely determined by the appropriate distance $r_{\alpha\beta}$ in a given molecular conformation, but not by all other sites (their influence is taken into account indirectly *via* a functional dependence of $\Delta\Psi_{\alpha\beta}$ on $w(r)$, *i.e.*, *via* the average equilibrium positions of other sites [23]). This is provided by a construction of $\Delta\Psi(\mathbf{r}_1, ..., \mathbf{r}_N)$: the procedure of averaging involves only coordinates of particles, whereas the coordinates of the molecule are taken as fixed. So, in accordance with this assumption, any pair of sites α and β of an N-site molecule at equilibrium can interact in a specific way, as compared with other site-site interactions in the molecule. Conclusions made on the basis of this statement are very significant to elucidate the situations where the so-called global conformational symmetry is broken. Grayce and Schweizer [23] analyze some relevant examples. Thus, in the case of collapsed polymer we have an equilibrium conformation, in which some monomers are on average placed inside the globule, while others are on average outside near the surface. As has been pointed out in reference [23], in this case the total medium-induced potential $\Delta\Psi(\mathbf{r}_1, ..., \mathbf{r}_N)$ can be written as a sum of the site-site contributions $\Delta\Psi_{\alpha\beta}$ without losing the distinction between the inside and outside monomers. This is due to the fact that the inside monomers move in a different potential field in comparison with the outside ones. This could be verified by using the results of our calculations presented in Figure 21 in the following way. Let us divide our globule into two parts: a dense core and a friable outer coat (shell). It is clear that the mean effective energy per monomeric unit in the core and in the shell is different (because of the difference in the environment). At small N, the fractions of the inside and outside monomers in the globule are nearly equal. However, as N increases, this ratio changes: the inside fraction becomes predominant. Consequently, the effective potential also must change and attain some limiting shape at large N. Such a tendency for $\Delta\Psi$ is indeed observed here (see Fig. 21).

We can clarify the role and the meaning of self-consistent determination of the medium-induced potential of mean force $\Psi(\mathbf{r}_1, ..., \mathbf{r}_N)$ regarding it as a functional of the averaged correlation function $w(\mathbf{r}_1, ..., \mathbf{r}_N)$ (or, inversely, the w determination as a functional of Ψ). It is worth-while to present the following simple reasoning. Let us suppose that there are no restrictions imposed on (maximum) bond length in our CBFM polymer chain; that is all monomers are regarded as non-bonded. In this case, we *actually* deal with a subsystem of N free particles. Nevertheless we will characterize the site-site correlations in this N-particle subsystem by the same function w as in the linked case, *i.e.*, we will *formally* regard these particles as belonging to the united set of N bonded interacting sites. On the other hand, from the *actual* viewpoint we have $\hat{w}_{\alpha\beta} = \delta_{\alpha\beta}$ (or, in terms of the PRISM approximation, $\hat{w}(q)) \equiv N^{-1} \sum_{\alpha,\beta} \hat{w}_{\alpha\beta} = 1$ at any q. We imply that the case in question corresponds to a bicomponent system in which the density of our "traced" N-particle subsystem $\rho_p \to 0$ (although it is not the strict limitation indeed). In addition, we restrict the subsystem of N particles by a very large but finite volume V (that provides the Fourier transform $w \to \hat{w}$). It is easy to understand that the results corresponding to the *actual* and *formal* considerations must be different. In the first case (when $\hat{w}_{\alpha\beta} = \delta_{\alpha\beta}$) the medium only renormalizes the bare potential, so that each site-site interaction contribution $\Psi_{\alpha\beta}$ to the full potential of mean force of the N-particle subsystem is given by

$$\Psi_{\alpha\beta} = -k_B T \ln[h_{pp'}(r_{\alpha\beta}) + 1] \tag{33}$$

where $h_{pp'}$ is found from equation (9). For an HNC-like closure we have simply

$$\begin{aligned} \Psi_{\alpha\beta} &= u_{pp'}(r_{\alpha\beta}) - k_B T \rho_d c_{pd} * h_{dp}(r_{\alpha\beta}) \\ &= u_{pp}(r_{\alpha\beta}) + k_B T[c_{pp'}(r_{\alpha\beta}) - h_{pp'}(r_{\alpha\beta}]. \end{aligned} \tag{34}$$

Note that these equations are valid for medium that consists of arbitrary particles (molecules). We can see that in the case under consideration no "third" particle γ belonging to the N-particle subsystem could interfere the interaction between any given pair of particles α and β. To be more correct, the equilibrium configuration probability distribution $\Omega_0(\mathbf{r}_1, ..., \mathbf{r}_N)$ of the set of N particles immersed in a medium is formed *without* "adjustments" of the particle coordinates and the effective potentials. On the other hand, if we consider the N-particle subsystem as an N-site *quasi-molecule*, the functions $\Psi_{\alpha\beta}$ and $\Omega(\mathbf{r}_1, ..., \mathbf{r}_N)$ are given by equations (18) and (16), which are functionals of $w(\mathbf{r}_1, ..., \mathbf{r}_N)$. For example, for $N = 2$, this gives $\hat{w}(q) = 1 + \sin(bq)/bq$, where b is some current (fixed) distance between the two particles ($\sigma_p < b < V^{1/3}$). Then, the medium-induced potential $\Delta\Psi_{12}$ depends parametrically on b through the two-site intramolecular correlation function $w(\mathbf{r}_1, \mathbf{r}_2)$; that is, $\Delta\Psi_{12} = \Delta\Psi_{12}(r; b)$. Solution of equation (8) for any given b gives the potential $\Delta\Psi_{12}$ averaged over all possible positions of medium particles. When b is large enough (namely, $b > \xi_d$ where ξ_d is the density-density correlation length in the medium), the constituent particles of our *quasi-molecule* do perturb environment independently. Otherwise, at $b < \xi_d$ the perturbed regions overlap and this may drastically alter the potential $\Delta\Psi_{12}$ in dense media [46]. In the case of free ("broken") particles, no such effects appear by definition. Regarding the one-dimensional parametrical dependence $\Delta\Psi_{12} = \Delta\Psi_{12}(r; b)$ we can readily find the equilibrium configuration probability distribution, $\Omega_0(\mathbf{r}_1, \mathbf{r}_2)$, or the equilibrium site-site distance, b_0. It should be recalled here that b is not an actual "chemical bond" but is a variational parameter in the quasi-molecular model under consideration. As usual, the equilibrium state is determined by the variational minimization of the Helmholtz free energy functional $\mathcal{F}[\Omega]$, *i.e.*, by the condition $\delta\mathcal{F}[\Omega_0]/\delta\Omega = 0$. In our case this is simply achieved by the minimization of the one-dimensional functional $\mathcal{F}[\Psi(b)]$. Note that the condition $\delta\mathcal{F}/\delta b = 0$ is a self-consistent equation, because $\mathcal{F}$

depends parametrically on b through $\Delta\Psi$. It is easily understood that minimization of $\mathcal{F}$ is equivalent to the Monte-Carlo sampling that is performed in the hybrid MC/RISM method. So, we see the principal difference between the two models: in the case of "free" particles, the shape of the potential surface $\Psi(\mathbf{r}_1, ..., \mathbf{r}_N)$ does not depend on a particular configuration of the traced N-particle subsystem. On the other hand, for the *quasi-molecular* model actual equilibrium shape of $\Psi(\mathbf{r}_1, ..., \mathbf{r}_N)$ is determined by the particular equilibrium configuration of N particles, or *vice versa*. It is reasonable to suppose that the difference pointed out here will be of importance in the theoretical treatment of condensed-phase effects.

We can explicitly find the contribution of interparticle interactions to the total effective potential in the *quasi-molecular* approach. To this end, we write the full potential as

$$\Psi_{\alpha\beta}/k_BT = \Psi^0_{\alpha\beta}/k_BT - \Psi^*_{\alpha\beta} \tag{35}$$

where $\Psi^0_{\alpha\beta}$ is the site-site effective potential of the free (unbounded) particles and $\Psi^*_{\alpha\beta}$ is the additional contribution due to the "bonding"-mediated correlations between particles (regardless to the reality of bonds). Equation (34) is valid for $\Psi^0_{\alpha\beta}$. By taking into account equation (12) and the RISM equations (7-9) it is possible to show that $\Psi^*_{\alpha\beta}$ is given by

$$\omega * \Psi^*_{\alpha\beta} * \omega = \rho h_{\alpha\beta}\rho - \omega * h_{\alpha\beta} * \omega \tag{36}$$

where $\omega = \rho w$. It is seen from equation (36) that $\Psi^* = 0$ at $w = 1$ or $N = 1$, as it must be. If $q \to 0$, then $\hat{\Psi}^*(0) \sim (N^{-2} - 1)$. Consequently, Ψ^* introduces maximum contribution into Ψ at large N and large distances. The Ψ^* dependence on N becomes weaker when N increases, as it is distinctively seen from Figure 21. Equation (36) serves as a good evidence that Ψ^* represents the influence of the indirect collective bonding-mediated correlations between particles. Just this contribution stipulates the additional effective attraction between particles in dense media with the "nonlocal" entropic effects being the incentive of this attraction.

Using the results of analysis of the self-consistent effective potentials, one may construct a hybrid simulation technique for modeling of multiple-chain systems. For this goal chains are to be treated as the units of a single complex "supermolecule". This "supermolecule" is described by a single united intramolecular site-site correlation function $\mathbf{W(r)}$ or (in the PRISM approximation) by single site-averaged correlation function $w(r)$.

There are some other examples directly related to the subject under discussion. In the Introduction, we have referred to the papers that predict the localized states of solvated electron in the framework of the RISM theory [15,16]. One more example of the entropy-driven effects is given in calculations by means of a simple (non-self-consistent) RISM approach for the athermal blends of rods and long Gaussian chains [47] and semiflexible chains with different aspect ratios [48]. As noted in reference [48], the contributions of volume changes to miscibility are due to entropic effects and can result in lower critical solution temperature (LCST) behavior in certain polymer alloys, as observed experimentally for polyolefin alloys [49,50] and the polystyrene/poly(n-butyl methacrylate) system [51]. One of the problems that illustrates the "attraction through repulsion" principle has been exactly solved. Frenkel and Louis [52] considered a simple two-dimensional lattice-gas model of binary mixture consisting of "small" and "large" hard-core particles. By transforming to a grand-canonical ensemble, this binary system with purely repulsive interactions can be mapped onto a one-component lattice-gas Ising model with attractive nearest-neighbor interaction between the "large" particles (squares). This lattice model can again be transformed to a two-dimensional Ising spin model solving in the case of zero external magnetic field. The phase behavior of such Ising-like models is known exactly [53,54]. The order-disorder transition in the Ising spin model corresponds to phase separation in the initial model. In this way Frenkel and Louis [52] observed the purely entropy-driven demixing transition in the square-lattice, hard-core mixture. Although our model corresponds to infinitely diluted system, nevertheless, it should manifest demixing of components provided appropriate parameters chosen.

Several other aspects of the problem discussed here are worth mentioning. Among them, the entropy effects influencing the local conformational structure of flexible molecules. Zichi and Rossky [55] and Talitskikh *et al.* [56] used the RISM integral equation theory to study molecular conformational equilibrium in solutions of small molecules with internal degrees of freedom. It was found that the average effect of solvent leads to appearance of the solvent-mediated torsional potential of a purely entropic nature. A second aspect covers the equilibrium and dynamical properties of chains in the so-called *disordered media*, where the particles of the media are spatially fixed impenetrable obstacles randomly distributed in two or three dimensions. By using Monte-Carlo simulations, it was shown that in this case the localization of chains occurs [57,58]. This means that, for entropic reasons, in larger holes one finds an increased density of chain units, as compared to the small holes. The understanding of conformational properties of chains in such media, when the material is percolated, is very important. In addition, while moving between fixed randomly distributed obstacles, a flexible polymer exhibits anomalous dynamical behavior [57]. It is quite necessary to take these facts into account in consideration of the static properties and dynamics of polymers within the framework of a model "polymer chain in an array of obstacles" [59–62].

5 Conclusion

Using the hybrid MC/RISM method, we have performed rather extensive studies of static properties of flexible polymer chains surrounded by colloidal particles with purely repulsive hard-core interactions between the particles and chain beads. It has been shown that the medium-induced collapse of a polymer may occur in such an athermal system, similar to a polymer collapse in a poor

solvent. Our analysis yields a simple "entropic" interpretation of this transition. We have presented the detailed study of the dependence of conformational properties of the chains on the degree of polymerization, density and size of colloidal particles. In general, our main results are in agreement with lattice computer simulations [12–14]. In addition, we have considered other closely related examples of entropy-driven transitions.

We thank K. Binder, K. Kremer, and G.S. Grest for helpful discussions. Financial support of the E.I. Du Pont de Nemours Company is gratefully acknowledged. This work was also supported by the Russian Foundation for Basic Researches (project # 98-03-33348).

References

1. D.H. Napper, *Polymeric Stabilization of Colloidal Dispersions* (Academic Press, London, 1983).
2. B. Vincent, J. Edwards, S. Emmet, R. Groot, Colloid Surf. **31**, 267 (1988).
3. P.G. Khalatur, Kolloid Zh. **46**, 294 (1984).
4. G.C.A.M. Mooij, D. Frenkel, Molec. Phys. **74**, 41 (1991).
5. D. Frenkel, Physica A **176**, 54 (1991).
6. D. Frenkel, *Advanced Monte-Carlo Techniques, in Computer Simulation in Chemical Physics*, edited by M.P. Allen, D.J. Tildesley (Kluwer Academic Publishers, 1993), pp. 93-152.
7. D. Frenkel, J. Phys. Cond. Mat. **2**, SA265 (1990).
8. E.J. Meijer, D. Frenkel, Phys. Rev. Lett. **67**, 1110 (1991)
9. P.G. Khalatur, L.V. Zherenkova, A.R. Khokhlov, J. Phys. II France **7**, 543 (1997); Physica A **247**, 205 (1997).
10. P.G. de Gennes, *Scaling Concepts in Polymer Physics* (Cornell University Press, Ithaca, 1979).
11. P. Fries, J.-P. Hansen, Molec. Phys. **48**, 891 (1983).
12. M. Dijkstra, D. Frenkel, Phys. Rev. Lett. **72**, 298 (1994).
13. M. Dijkstra, D. Frenkel, J.-P. Hansen, J. Chem. Phys. **101**, 3179 (1994).
14. G. Luna-Barcenas, G.E. Bennett, I.C. Sanchez, K.P. Johnston, J. Chem. Phys. **104**, 9971 (1996).
15. D. Chandler, Y. Singh, D.M. Richardson, J. Chem. Phys. **81**, 1975 (1984).
16. A.L. Nichols, D. Chandler, Y. Singh, D.M. Richardson, J. Chem. Phys. **81**, 5109, (1984).
17. L.R. Pratt, D. Chandler, J. Chem. Phys. **66**, 147 (1977); D. Chandler, L.R. Pratt, J. Chem. Phys. **65**, 2925 (1976).
18. Y. Singh, J. Phys. A **20**, 3949 (1987).
19. S.J. Singer, D. Chandler, Molec. Phys. **55**, 621 (1085).
20. M. Sprik, M.L. Klein, D. Chandler, J. Chem. Phys. **83**, 3042 (1985).
21. D. Hsu, D. Chandler, J. Chem. Phys. **93**, 5075, (1990).
22. D. Laria, D. Wu, D. Chandler, J. Chem. Phys. **95**, 4444 (1991).
23. C.J. Grayce, K.S. Schweizer, J. Chem. Phys. **100**, 6846 (1994).
24. K.S. Schweizer, K.G. Honnell, J.G. Curro, J. Chem. Phys. **96**, 3211 (1992).
25. J. Melenkevitz, J.G. Curro, K.S. Schweizer, J. Chem. Phys. **99**, 5571 (1993).
26. C.J. Grayce, A. Yethiraj, K.S. Schweizer, J. Chem. Phys. **100**, 6857 (1994).
27. S.K. Talitskikh, P.G. Khalatur, Russ. J. Phys. Chem. **67**, 412 (1993); P.G. Khalatur, S.K. Talitskikh, A.V. Krupko, in *Computational Methods in Chemistry* (Tver State University Press, Tver, 1990), p.90.
28. J. Melenkevitz, K.S. Schweizer, J.G. Curro, Macromol. **26**, 6190 (1993).
29. P.G. Khalatur, Russ. Phys. Bull. **59**, 178 (1995).
30. S.K. Talitskikh, Ph.D. thesis, Tver State University, 1993.
31. A. Alavi, D. Frenkel, J. Chem. Phys. **97**, 9249 (1992).
32. T. Biben, J.-P. Hansen, Phys. Rev. Lett. **66**, 2215 (1991).
33. D. Chandler, H.C. Anderson, J. Chem. Phys. **57**, 1917 (1972).
34. D. Chandler, H.C. Anderson, J. Chem. Phys. **57**, 1930 (1972).
35. D. Chandler, in *Studies in Statistical Mechanics*, edited by E.W. Montroll, J.L. Lebowitz, (North-Holland, Amsterdam), Vol. 8, p. 274.
36. J.G. Curro, K.S. Schweizer, Macromol. **20**, 1928 (1987).
37. K.S. Schweizer, J.G. Curro, Phys. Rev. Lett. **58**, 256 (1987).
38. K.S. Schweizer, J.G. Curro, Adv. Polym. Sci. **116**, 319 (1994).
39. S.K. Talitskikh, P.G. Khalatur, Russ. J. Phys. Chem. **69**, 9 (1995); *ibid.* **69**, 264 (1995).
40. I.M. Lifshitz, A.Yu. Grosberg, A.R. Khokhlov, Rev. Mod. Phys. **50**, 683 (1978).
41. A.Yu. Grosberg, A.R. Khokhlov, *Statistical Physics of Macromolecules* (American Institute of Physics, New York, 1994).
42. S.K. Talitskikh, P.G. Khalatur, Russ. J. Phys. Chem. **69**, 2 (1995); I.V. Makeeva, V.G. Kokacheva, S.K. Talitskikh, P.G. Khalatur, Russ. J. Struct. Chem. **36**, 799 (1995).
43. P. Ballone, G. Pastore, G. Galli, D. Gazzillo, Molec. Phys. **59**, 275 (1986).
44. C.J. Grayce, J. Chem. Phys. **106**, 5171 (1997).
45. P.G. Khalatur, A.R. Khokhlov, Molec. Phys. **93**, 555 (1998).
46. L.R. Pratt, D. Chandler, J. Chem. Phys. **65**, 2925 (1976); **67**, 3683 (1977).
47. J.D. Honeycutt, Amer. Chem. Soc. Polymer Prepr. **33** (1), 529 (1992).
48. K.S. Schweizer, C. Singh, Macromol. **28**, 2063 (1995).
49. D.J. Walsh, W.W. Graessley, S. Datta, D.J. Lohse, L.J. Fetters, Macromol. **25**, 5236 (1992).
50. W.W. Graessley, R. Krishnamoorti, N.P. Balsara, R.J. Butera, L.J. Fetters, D.J. Lohse, D.N. Schulz, J.A. Sissano, Macromol. **27**, 3896 (1994).
51. B. Hammouda, B.J. Bauer, T.P. Russell, Macromol. **27**, 2357 (1994).
52. D.Frenkel, A.A. Louis, Phys. Rev. Lett. **68**, 3365 (1992).
53. L. Onsager, Phys. Rev. **65**, 117 (1944).
54. T.D. Lee, C.N. Yang, Phys. Rev. **87**, 410 (1952).
55. D.A. Zichi, P.J. Rossky, J. Chem. Phys. **84**, 1712 (1986).
56. S.K. Talitskikh, I.V. Makeeva, P.G. Khalatur, Russ. J. Phys. Chem. **68**, 1282 (1994).
57. A. Baumgärtner, Europhys. Lett. **4**, 122 (1987).
58. A. Baumgärtner, M. Muthukumar, J. Chem. Phys. **87**, 3082 (1987).
59. E. Helfand, D.S. Pearson, J. Chem. Phys. **79**, 2054 (1983).
60. A.R. Khokhlov, S.K. Nechaev, Phys. Lett. A **112**, 156 (1985).
61. M. Rubinstein, E. Helfand, J. Chem. Phys. **82**, 2477 (1985).
62. A.R. Khokhlov, F.F. Ternovsky, E.A. Zheligovskaya, Physica A **163**, 747 (1990).